ISSN (Online): 2583-648X

IJIRID

International Journal of Ingenious Research, Invention and Development

An International, High Impact Factor, Double-Blind Peer-Reviewed, Open-Access, Multidisciplinary Online Journal

www.ijirid.in

Volume 5 | Issue 4 | August 2026

VLSI-Accelerated Chest X-Ray Image Segmentation using Adaptive Hybrid Clustering: MATLAB–FPGA Co-Design and Performance Evaluation

M. Shobha Rani[1], A. Baloji[2], Bandari Gunavardhan[3]

[1,2]*Assistant Professor, Dept. of ECE, Brilliant Grammar School Educational Society's Group of Institutions, Hyderabad, India*

[3]*Dept. of ECE, Brilliant Grammar School Educational Society's Group of Institutions, Hyderabad, India*

Abstract: *Chest X-ray segmentation is a fundamental preprocessing stage for computer-aided analysis of pulmonary disease, but software-only segmentation can become a bottleneck when low latency and embedded execution are required. This paper presents a MATLAB–VLSI co-design for chest X-ray image segmentation using the hybrid clustering procedure described in the supplied implementation. The processing chain reads a chest X-ray image in MATLAB, converts it to grayscale, forms a text-based numerical representation, and sends the pixel data to a hardware-oriented hybrid clustering core. The hybrid method performs automated cluster-count selection, cluster-to-cluster similarity analysis, internal pixel-difference analysis, cluster merging/reduction to two principal regions, maximum-pixel-based region finalization, and generation of an output text file that is reconstructed as a segmented image in MATLAB. The design is implemented and evaluated using Xilinx Vivado with a Zynq-7000 target. Three sample chest X-ray images are reported in the source evaluation. The baseline K-means implementation produces average accuracy, Dice coefficient, and Jaccard index values of 70.494%, 50.8043%, and 38.8676%, respectively, whereas the proposed method reports 99.9959%, 99.9921%, and 99.9842%. FPGA results show a reduction in LUT utilization from 36 to 29 and I/O utilization from 96 to 94. The proposed implementation reports 21.216 W dynamic power and 0.485 W static power, compared with 30.326 W and 4.528 W for the baseline. These results demonstrate the potential of hybrid clustering combined with hardware acceleration for low-latency medical-image segmentation, while also highlighting the need for broader dataset validation and standardized ground-truth evaluation.*

Keywords: Chest X-ray, Image Segmentation, VLSI, FPGA, Hybrid Clustering, K-means, Medical Imaging, MATLAB, Vivado, Zynq-7000.

I. Introduction

Chest radiography is among the most widely used imaging modalities for screening and diagnosis of thoracic disease because it is fast, relatively inexpensive, and broadly available. Segmentation of the lung fields and other anatomical regions is often required before quantitative analysis, computer-aided diagnosis, disease localization, or downstream classification. In an automated workflow, segmentation reduces irrelevant background structures and can focus subsequent algorithms on clinically meaningful regions. The computational challenge becomes important when segmentation is expected to operate in telemedicine, portable diagnostic equipment, or real-time medical-imaging systems. Software implementations provide flexibility, but iterative clustering and pixel-level

 DOI: 10.5281/zenodo.22755101

ISSN (Online): 2583-648X
IJIRID
International Journal of Ingenious Research, Invention and Development
An International, High Impact Factor, Double-Blind Peer-Reviewed, Open-Access, Multidisciplinary Online Journal
Volume 5 | Issue 4 | August 2026
www.ijirid.in

processing can introduce latency and high computational overhead. The supplied project therefore investigates hardware acceleration of chest X-ray segmentation using a VLSI-oriented implementation. Its motivation is to transfer repetitive pixel processing from software to dedicated hardware, where parallel and fixed-function arithmetic can reduce delay and resource demand.

The baseline method in the supplied implementation is K-means segmentation. K-means groups pixels according to intensity similarity and is attractive because of its simplicity, but its performance depends on the selected number of clusters and initialization, and it can be sensitive to intensity variation and irregular anatomical boundaries. The proposed approach replaces this fixed clustering behavior with a hybrid procedure that automatically selects the number of clusters, compares clusters for similarity, analyzes within-cluster pixel differences, reduces the segmentation to two final regions, and finalizes regions according to dominant pixel values.

This paper reformulates the supplied thesis-scale implementation into a journal-style study focused on the algorithm–hardware co-design, the FPGA realization, and the reported segmentation and hardware results. The work does not introduce a new dataset beyond the three sample images reported in the source; instead, it documents the architecture and the measured comparison between the existing and proposed implementations.

1.1 Main Contributions

- A MATLAB–VLSI processing chain that converts chest X-ray pixel data into a hardware-consumable representation and reconstructs the segmented result.
- An adaptive hybrid clustering workflow with automated cluster-count selection, cluster similarity analysis, pixel-level internal analysis, cluster reduction, and region finalization.
- An FPGA implementation targeting a Zynq-7000 device and evaluated using LUT, I/O, delay, and power metrics.
- A direct comparison with the source baseline K-means method using eight segmentation metrics and three chest X-ray samples.
- A consolidated discussion of the reported results, including implementation limitations and reporting inconsistencies that should be addressed in future validation.

II. Related Work and Research Gap

Research on chest X-ray analysis spans threshold segmentation, clustering, convolutional neural networks, U-Net variants, attention-based segmentation, optimization-assisted multilevel thresholding, and hybrid segmentation–classification frameworks. Song et al. reported spectral clustering for chest-disease X-ray classification and showed advantages over pure K-means in the studied setting [1]. Al-Zyoud et al. used threshold-based segmentation for COVID-19 chest X-ray analysis [2], illustrating the continued relevance of low-complexity segmentation when computational resources are constrained.

Deep-learning approaches dominate recent segmentation studies. Chakraborty et al. investigated U-Net variants for COVID-19 infection localization [3], while Wahyuningrum et al. used attention-enhanced FCA-Net for lung segmentation [6]. Gopatoti and Vijayalakshmi optimized SegNet/U-Net-

 DOI: 10.5281/zenodo.22755101

ISSN (Online): 2583-648X

IJIRID

International Journal of Ingenious Research, Invention and Development

An International, High Impact Factor, Double-Blind Peer-Reviewed, Open-Access, Multidisciplinary Online Journal

Volume 5 | Issue 4 | August 2026

www.ijirid.in

based semantic segmentation networks for COVID-19 [7]. Gómez et al. addressed high-resolution multi-organ segmentation and reported strong Dice performance without severe down-sampling [8]. Gite et al. studied enhanced lung segmentation and the benefit of segmentation before disease classification [9].

Other studies have combined optimization and hybrid strategies with medical-image segmentation. Chen et al. applied a dynamic mechanism-assisted artificial bee colony method to multithreshold COVID-19 X-ray segmentation [10]. Iqbal et al. coupled lung segmentation with a classification pipeline for tuberculosis [11]. Priya et al. used fuzzy-entropic segmentation and differential evolution [16], and Hao et al. investigated an enhanced fruit-fly optimizer for multithreshold segmentation [20]. These methods emphasize segmentation quality but can introduce substantial computational cost.

The source project identifies a hardware-oriented research gap: segmentation methods that achieve high reported accuracy may be computationally intensive, whereas simple methods such as fixed K-means can be hardware-friendly but less robust to intensity variability and non-linear structures. The proposed system therefore seeks a middle ground—a clustering-based method with adaptive cluster handling, mapped to a compact VLSI/FPGA flow rather than a large deep neural network.

III. Proposed MATLAB–VLSI Hybrid-Clustering Methodology

The proposed architecture is organized as a co-design in which MATLAB performs image acquisition, grayscale conversion, numerical/text representation, and final reconstruction, while the VLSI core executes the hybrid clustering stage. This division keeps file-format and visualization tasks in software and places the repetitive clustering operations in hardware.

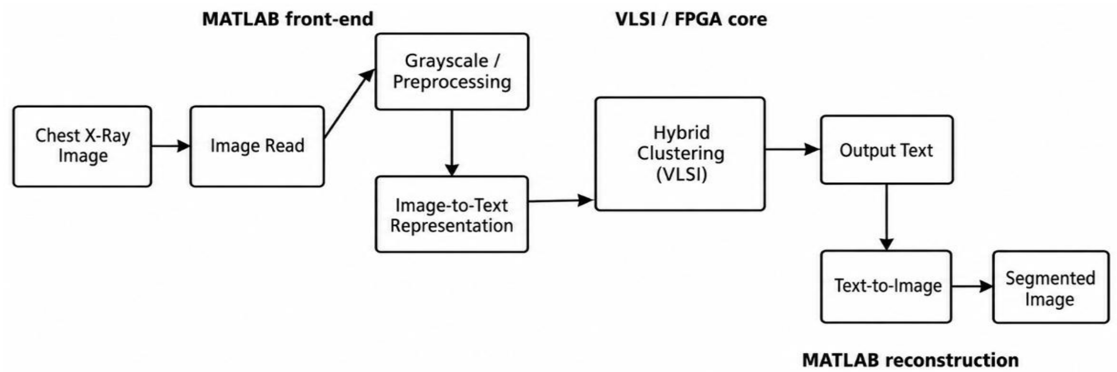

Figure 1: MATLAB–VLSI co-design used for the proposed chest X-ray segmentation system

3.1 MATLAB Front-End and Data Conversion: A chest X-ray image is first read in MATLAB and converted to grayscale when required. The source document describes preprocessing for image-quality enhancement and noise reduction before conversion of the image information into a text-based representation. This representation serves as the interface to the VLSI implementation. After clustering, the hardware produces output text data, which MATLAB converts back to image form to obtain the segmented chest X-ray.

DOI: 10.5281/zenodo.22755101

ISSN (Online): 2583-648X

IJIRID

International Journal of Ingenious Research, Invention and Development

An International, High Impact Factor, Double-Blind Peer-Reviewed, Open-Access, Multidisciplinary Online Journal

Volume 5 | Issue 4 | August 2026

www.ijirid.in

3.2 Hybrid Clustering Procedure: The source frames the proposed method as a hybrid of clustering concepts including K-means, hierarchical clustering, and density-oriented grouping. The implemented procedure itself is specified through seven sequential operations rather through a single named mathematical clustering algorithm. The operations are summarized below.

Table 1: Hybrid clustering operations described in the supplied implementation

Step	Operation	Function
1	Pixel acquisition and storage	Read input pixel values and retain their spatial/intensity information in memory.
2	Automatic cluster-count selection	Adapt the number of clusters to the amount of variation observed in the image.
3	Cluster-to-cluster similarity analysis	Compare clusters; merge similar or overlapping clusters while preserving dissimilar ones.
4	Internal cluster/pixel analysis	Estimate pixel-to-pixel differences inside clusters to check homogeneity and identify distinct regions.
5	Two-cluster generation	Reduce the set of clusters to two principal regions suitable for binary segmentation.
6	Region finalization	Use maximum/dominant pixel values to finalize regions and increase separation between normal and affected areas.
7	Output generation	Write the segmented cluster assignments/result into an output text file for reconstruction in MATLAB.

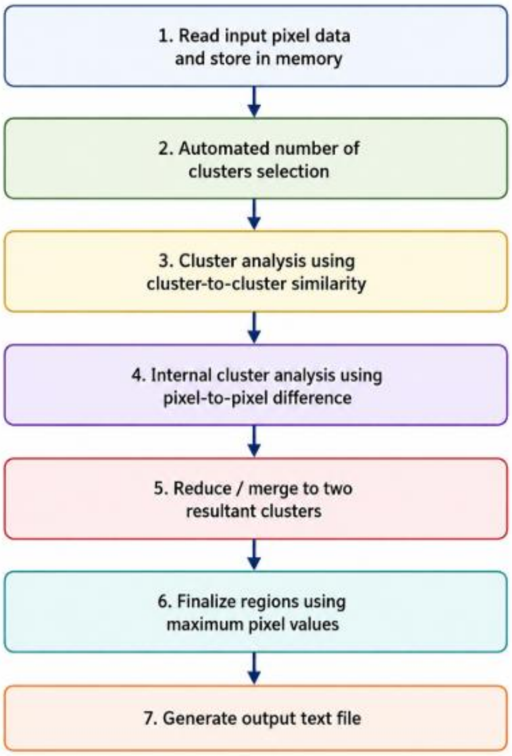

Figure 2: Hardware-oriented hybrid clustering workflow

ISSN (Online): 2583-648X

IJIRID

International Journal of Ingenious Research, Invention and Development

An International, High Impact Factor, Double-Blind Peer-Reviewed, Open-Access, Multidisciplinary Online Journal

Volume 5 | Issue 4 | August 2026

www.ijirid.in

3.3 Interpretation of the Cluster-Reduction Logic: The adaptive cluster-count stage avoids fixing a single value of K for every image. When the image contains greater variation, more intermediate clusters can be retained; when variation is smaller, fewer clusters are required. This is intended to improve adaptability compared with the existing fixed K-means segmentation.

After initial grouping, cluster-to-cluster similarity is evaluated. Similar clusters are merged so that redundant or overlapping regions do not persist through the complete processing path. The next stage examines pixel variation inside each cluster to determine whether a cluster is internally coherent or contains substantially different pixel values. The processing is finally reduced to two principal output regions. The finalization step emphasizes maximum pixel-value differences so that the resulting binary segmentation produces visually distinct foreground/background regions. The final cluster assignments are exported as text data for image reconstruction.

IV. FPGA/VLSI Implementation and Experimental Setup

4.1 Target Platform: The source implementation uses Xilinx Vivado and identifies a Zynq-7000 device as the target. The device attributes reported in the project setup are given in Table 2.

Table 2: FPGA target used in the supplied Vivado implementation

Attribute	Reported value
Part number	xc7z007sclg400-1
Family	Zynq-7000
Package	clg400
Speed grade	-1
Temperature grade	C

The hardware simulation uses 32-bit file-oriented input/output signals. The source waveform identifies input_file1[31:0] and input_file2[31:0] as the input data representations and output_file[31:0] as the resulting segmented output. The hardware report evaluates logic utilization, I/O utilization, setup and hold timing, and dynamic/static power.

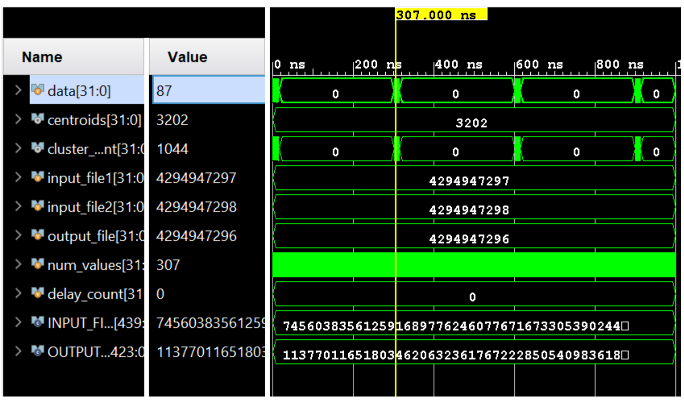

Figure 3: Vivado simulation of the proposed VLSI clustering implementation (source output)

ISSN (Online): 2583-648X

IJIRID

International Journal of Ingenious Research, Invention and Development

An International, High Impact Factor, Double-Blind Peer-Reviewed, Open-Access, Multidisciplinary Online Journal

Volume 5 | Issue 4 | August 2026

www.ijirid.in

4.2 Segmentation Evaluation Metrics: The source evaluates segmentation using accuracy, sensitivity, precision, F-measure, Matthews correlation coefficient (MCC), Dice coefficient, Jaccard index, and specificity. For a binary segmentation with true positive (TP), true negative (TN), false positive (FP), and false negative (FN) pixels, the commonly used forms corresponding to the definitions in the source are:

$$Accuracy = \frac{(TP + TN)}{(TP + TN + FP + FN)}$$

$$Sensitivity = \frac{TP}{(TP + FN)}$$

$$Precision = \frac{TP}{(TP + FP)}$$

$$F1\ (F - measure) = 2 \times Precision \times \frac{Sensitivity}{(Precision + Sensitivity)}$$

$$Dice = \frac{2TP}{(2TP + FP + FN)}$$

$$Jaccard = \frac{TP}{(TP + FP + FN)}$$

$$Specificity = \frac{TN}{(TN + FP)}$$

$$MCC = \frac{(TP \cdot TN - FP \cdot FN)}{\sqrt{[(TP + FP)(TP + FN)(TN + FP)(TN + FN)]}}$$

The source also discusses PSNR and SSIM in the problem statement, but the final results chapter does not report numerical PSNR or SSIM values. Consequently, they are not included in the quantitative comparison presented here.

V. Results and Discussion

5.1 Qualitative Segmentation Results: The supplied evaluation contains three representative chest X-ray images. The existing K-means method shows large variations in the segmented lung regions, including missing boundaries and substantial non-lung areas. The proposed outputs show cleaner two-region lung masks for all three samples. Figure 4 consolidates the source result images for direct visual comparison.

 DOI: 10.5281/zenodo.22755101

ISSN (Online): 2583-648X
IJIRID
International Journal of Ingenious Research, Invention and Development
An International, High Impact Factor, Double-Blind Peer-Reviewed, Open-Access, Multidisciplinary Online Journal
Volume 5 | Issue 4 | August 2026
www.ijirid.in

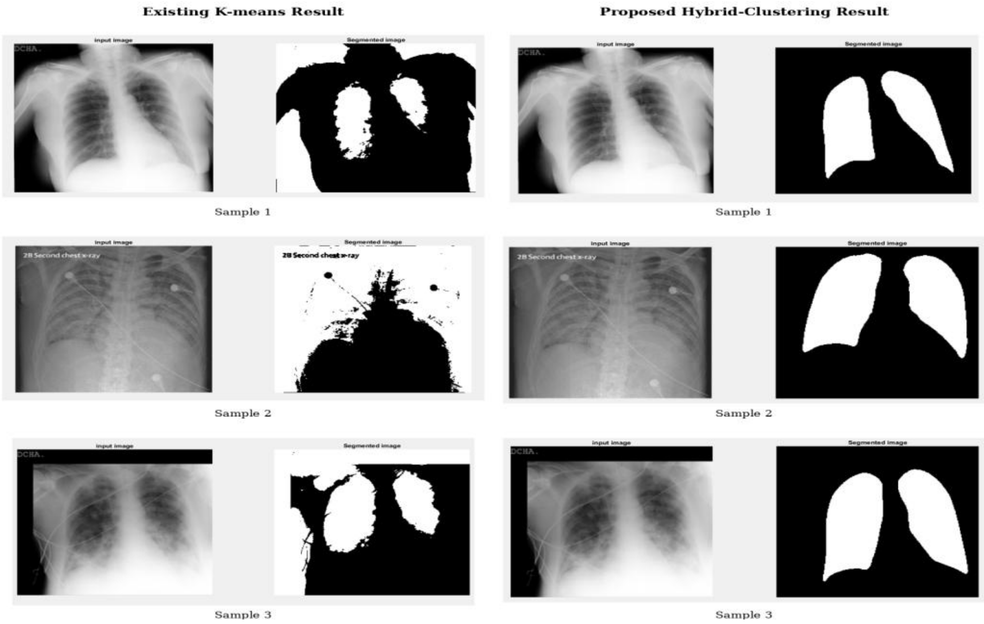

Figure 4: Existing K-means and proposed hybrid-clustering segmentation results for the three source *samples.*

5.2 Quantitative Segmentation Performance:

Table 3: Existing K-means segmentation results reported for the three samples

Metric	Sample 1	Sample 2	Sample 3	Average
Accuracy	65.9288	81.3772	64.176	70.494
Sensitivity	10.1212	76.38	47.7671	44.7561
F-measure	15.2004	83.4751	53.7376	50.8043
Precision	30.513	92.0234	61.4138	61.3167
MCC	0.24863	63.9945	25.7778	30.0069
Dice	15.2004	83.4751	53.7376	50.8043
Jaccard	8.2254	71.6371	36.7405	38.8676
Specificity	90.0413	89.3874	76.8391	85.4226

Table 4: Proposed hybrid-clustering segmentation results reported for the three samples

Metric	Sample 1	Sample 2	Sample 3	Average
Accuracy	99.9939	99.9985	99.9954	99.9959
Sensitivity	100	100	99.9895	99.9965
F-measure	99.9868	99.9974	99.9921	99.9921
Precision	99.9735	99.9948	99.9948	99.9877
MCC	99.9828	99.9963	99.9889	99.9893

ISSN (Online): 2583-648X

IJIRID

International Journal of Ingenious Research, Invention and Development

An International, High Impact Factor, Double-Blind Peer-Reviewed, Open-Access, Multidisciplinary Online Journal

Volume 5 | Issue 4 | August 2026

www.ijirid.in

Dice	99.9868	99.9974	99.9921	99.9921
Jaccard	99.9735	99.9948	99.9843	99.9842
Specificity	99.9921	99.9978	99.9978	99.9959

The average values show a large separation between the baseline and proposed implementations. Average accuracy increases from 70.494% to 99.9959%, sensitivity from 44.7561% to 99.9965%, Dice coefficient from 50.8043% to 99.9921%, and Jaccard index from 38.8676% to 99.9842%. The MCC also rises from 30.0069% to 99.9893%. Within the supplied three-sample experiment, the proposed outputs are therefore highly consistent across the reported pixel-level metrics.

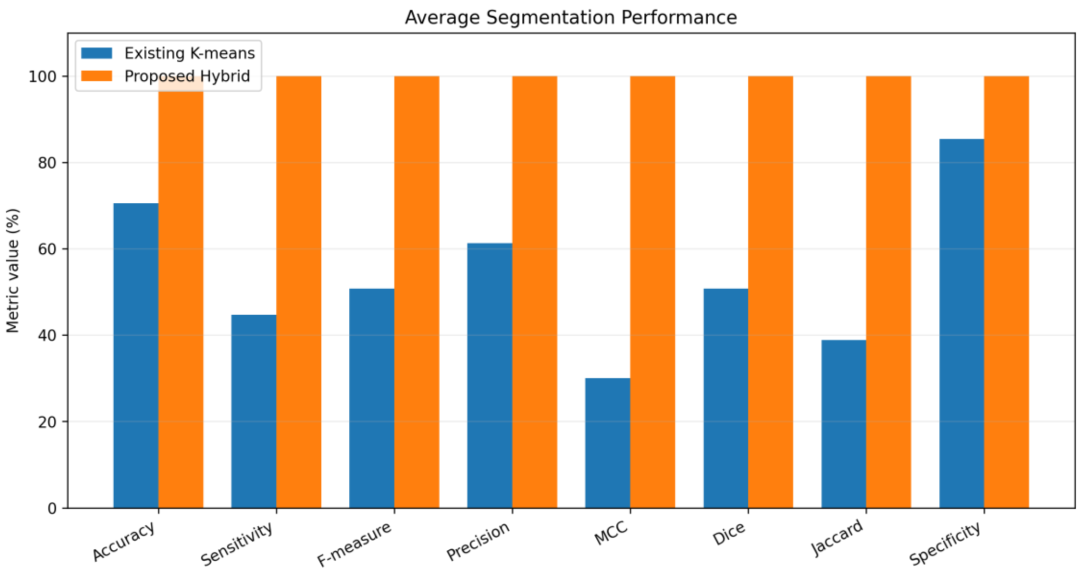

Figure 5: Average segmentation metrics reported for the existing and proposed methods

Table 5: Average MATLAB segmentation comparison reproduced from the source results

Metric	Existing Method	Proposed Method
Accuracy	70.494	99.9959
Sensitivity	44.7561	99.9965
F-measure	50.8043	99.9921
Precision	61.3167	99.9877
MCC	30.0069	99.9893
Dice	50.8043	99.9921
Jaccard	38.8676	99.9842
Specificity	85.4226	99.9959

 DOI: 10.5281/zenodo.22755101

ISSN (Online): 2583-648X

IJIRID

International Journal of Ingenious Research, Invention and Development

An International, High Impact Factor, Double-Blind Peer-Reviewed, Open-Access, Multidisciplinary Online Journal

Volume 5 | Issue 4 | August 2026

www.ijirid.in

5.3 FPGA Resource, Power, and Timing Results: The proposed synthesis report uses 29 LUTs out of 32,600 available LUTs (0.09%) and 94 I/O resources out of 150 (62.67%). The source reports 21.216 W of dynamic power, including 1.178 W signal power, 0.109 W logic power, and 19.929 W I/O power, together with 0.485 W static power. The proposed setup report lists 10.709 ns total delay, 4.761 ns logic delay, and 5.947 ns net delay; the proposed hold report lists 3.748 ns total delay, 1.534 ns logic delay, and 2.214 ns net delay.

Table 6: VLSI/FPGA performance comparison as tabulated in the source document

Hardware Metric	Existing Method	Proposed Method
LUT	36	29
I/O	96	94
Setup logic delay (ns)	15.678	4.761
Setup net delay (ns)	16.867	5.947
Setup total delay (ns)	23.897	10.709
Hold logic delay (ns)	3.457	1.534
Hold net delay (ns)	4.576	2.214
Hold total delay (ns)	6.899	3.748
Dynamic power (W)	30.326	21.216
Static power (W)	4.528	0.485

Using the tabulated total-delay values, the proposed design reduces LUT use by 19.44%, I/O use by 2.08%, setup total delay by approximately 55.18%, hold total delay by 45.67%, dynamic power by 30.04%, and static power by 89.29%. These reductions indicate that the hybrid-clustering implementation is not only more accurate in the reported MATLAB evaluation but also more compact and power-efficient in the reported FPGA comparison.

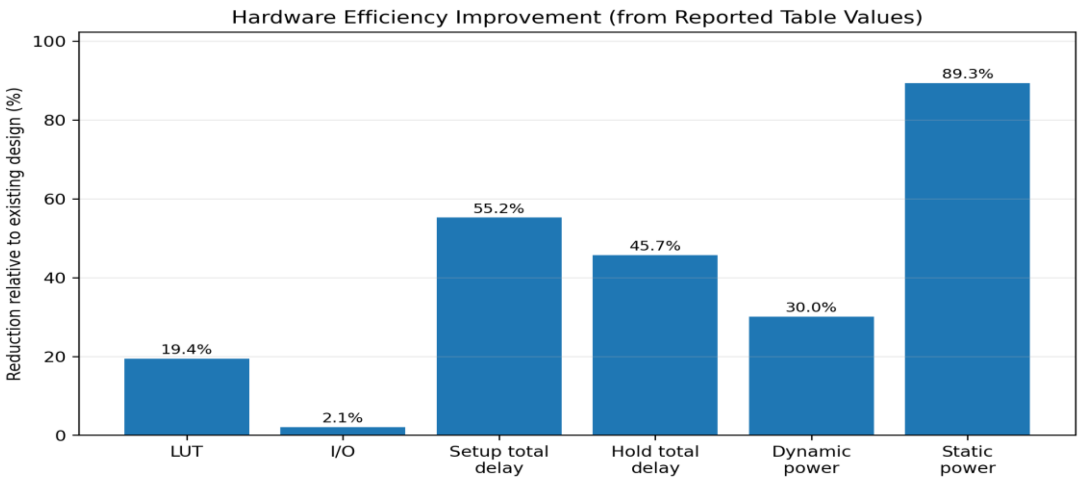

Figure 6: Hardware-efficiency reduction calculated from the source table values

DOI: 10.5281/zenodo.22755101

ISSN (Online): 2583-648X

IJIRID

International Journal of Ingenious Research, Invention and Development

An International, High Impact Factor, Double-Blind Peer-Reviewed, Open-Access, Multidisciplinary Online Journal

Volume 5 | Issue 4 | August 2026

www.ijirid.in

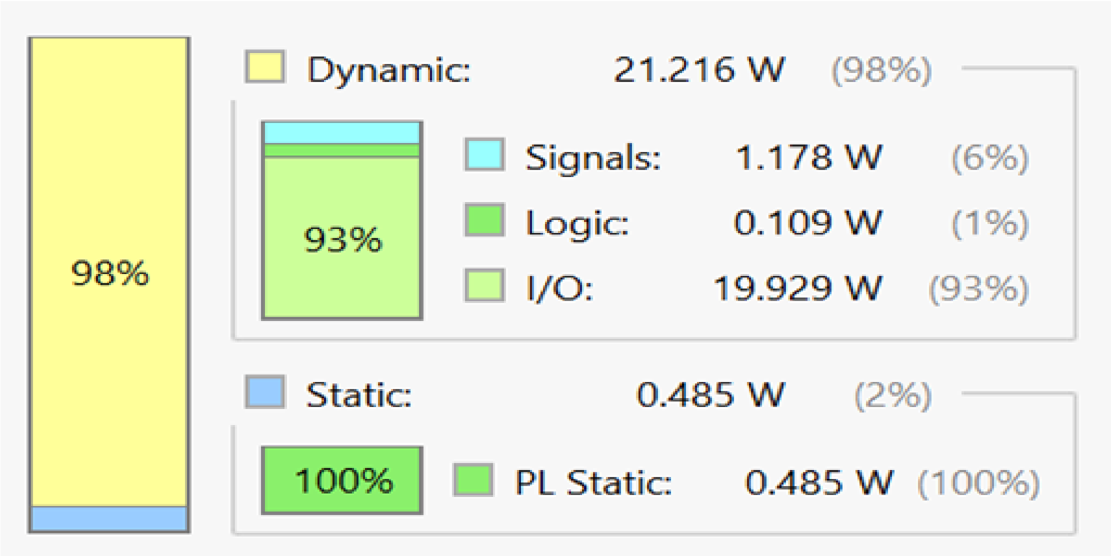

Figure 7: Vivado power report for the proposed implementation (source output)

5.4 Discussion: The most important algorithmic difference from the baseline is the adaptive treatment of cluster structure. Fixed K-means can force every image into a predetermined number of intensity groups even when the amount of image variation changes substantially. In the proposed procedure, the number of clusters can vary initially, and similarity-based merging reduces redundant groups before the final binary segmentation. This mechanism is consistent with the cleaner lung masks visible in the three supplied samples.

The hardware results suggest that the adaptive algorithm does not necessarily require a larger FPGA footprint in the reported implementation. The LUT count falls from 36 to 29, while the reported dynamic and static power also decrease. The largest power component of the proposed report is I/O power (19.929 W), indicating that data movement and interface activity dominate the estimated dynamic power. Future implementations should therefore consider more compact streaming or on-chip memory interfaces if system-level energy is a priority.

The segmentation metrics reported by the source are exceptionally high for the three proposed samples, with all averages above 99.98%. These values demonstrate strong consistency within the supplied evaluation, but the source does not identify a named dataset, the number of independently annotated ground-truth masks beyond the three examples, or a cross-validation protocol. Consequently, the reported values should be interpreted as implementation-level results for the supplied samples rather than as a population-level clinical performance estimate.

Reporting note: *the narrative text accompanying Table 7.7 in the source describes the existing setup total delay as 15.678 ns, while the table itself lists the setup entries as 15.678 ns logic delay, 16.867 ns net delay, and 23.897 ns total delay. This paper reproduces the tabulated values and explicitly retains this source-level discrepancy rather than silently reconciling it.*

 DOI: 10.5281/zenodo.22755101

ISSN (Online): 2583-648X

IJIRID

International Journal of Ingenious Research, Invention and Development

An International, High Impact Factor, Double-Blind Peer-Reviewed, Open-Access, Multidisciplinary Online Journal

Volume 5 | Issue 4 | August 2026

www.ijirid.in

VI. Applications, Limitations, and Future Scope

6.1 Potential Applications

- Real-time lung-field segmentation before computer-aided chest-disease analysis.
- Portable or point-of-care imaging systems where dedicated FPGA logic can reduce software workload.
- Telemedicine and remote healthcare platforms requiring rapid preprocessing before image transmission or diagnosis.
- Preprocessing for pneumonia, COVID-19, tuberculosis, lung-cancer, and other thoracic disease analysis, subject to task-specific clinical validation.
- Hardware-accelerated preprocessing stages for larger AI pipelines in which segmentation is performed before classification.

6.2 Current Limitations

- The source evaluation reports only three representative chest X-ray samples and does not specify a named benchmark dataset or a complete ground-truth annotation protocol.
- The exact mathematical rule used for automated cluster-count selection and the threshold used for cluster similarity merging are not specified in the source; therefore, the architecture is reproducible at the functional-flow level but not fully parameterized from the document.
- PSNR and SSIM are discussed as image-quality considerations in the source but are not reported numerically in the final results.
- The power values are Vivado estimates and depend on activity assumptions, device configuration, clocking, and I/O behavior; they should not be treated as direct board-level measurements unless independently verified.
- Clinical usefulness requires validation on substantially larger and heterogeneous datasets before deployment.

6.3 Future Work

- Optimize cluster similarity and pixel-difference blocks for deeper parallelism and streaming image input.
- Reduce I/O-dominated power through on-chip buffering, data-width optimization, clock gating, and more efficient memory interfaces.
- Validate the hybrid method on public chest X-ray segmentation datasets with expert ground-truth masks and standardized train/test protocols.
- Integrate lightweight CNN or U-Net features with the hybrid clustering core while retaining FPGA-friendly complexity.
- Extend the method to CT and MRI segmentation and study domain adaptation across acquisition devices.
- Investigate privacy-preserving and secure medical-image processing for telemedicine deployments.

ISSN (Online): 2583-648X

IJIRID

International Journal of Ingenious Research, Invention and Development

An International, High Impact Factor, Double-Blind Peer-Reviewed, Open-Access, Multidisciplinary Online Journal

Volume 5 | Issue 4 | August 2026

www.ijirid.in

VII. Conclusion

A VLSI-accelerated chest X-ray segmentation system based on adaptive hybrid clustering has been presented from the supplied implementation. The design divides the processing between MATLAB and a hardware clustering core: MATLAB performs image acquisition, grayscale conversion, data representation, and reconstruction, while the VLSI stage performs automated cluster-count selection, similarity-based cluster analysis, internal pixel-difference analysis, cluster reduction, and region finalization. The reported three-image evaluation shows a substantial improvement over the existing K-means method, with average accuracy increasing from 70.494% to 99.9959%, Dice from 50.8043% to 99.9921%, and Jaccard from 38.8676% to 99.9842%. The source FPGA comparison also reports lower LUT use, lower delay, and lower dynamic/static power for the proposed design. These results support the feasibility of a hardware-oriented clustering pipeline for rapid chest X-ray segmentation. Broader dataset validation, explicit specification of adaptive clustering thresholds, and power-optimized streaming interfaces are the main next steps needed to move the design from a proof-of-concept implementation toward a reproducible clinical-grade accelerator.

References

[1] W. Al-Zyoud, D. Erekat, and R. Saraiji, “COVID-19 chest X-ray image analysis by threshold-based segmentation,” Heliyon, vol. 9, no. 3, 2023.

[2] G. S. Chakraborty, S. Batra, and M. Mahajan, “A novel deep learning-based approach for COVID-19 infection identification in chest X-ray image using improved image segmentation technique,” in Proc. IEEE ICOEI, pp. 1102–1109, 2023.

[3] L. Liu and Y. Yin, “Towards explainable AI on chest X-ray diagnosis using image segmentation and CAM visualization,” in Proc. Future of Information and Communication Conf., pp. 659–675, 2023.

[4] Md. Javeed and G. Kande, “A survey on linking of cell tracks using segmentation,” International Journal of Applied Engineering Research, vol. 13, no. 7, pp. 5183–5189, 2018.

[5] R. T. Wahyuningrum et al., “Improvement of chest X-ray image segmentation accuracy based on FCA-Net,” Cogent Engineering, vol. 10, no. 1, Art. no. 2229571, 2023.

[6] A. Gopatoti and P. Vijayalakshmi, “Optimized chest X-ray image semantic segmentation networks for COVID-19 early detection,” Journal of X-Ray Science and Technology, vol. 30, no. 3, pp. 491–512, 2022.

[7] O. Gómez, P. Mesejo, O. Ibáñez, A. Valsecchi, and O. Cordón, “Deep architectures for high-resolution multi-organ chest X-ray image segmentation,” Neural Computing and Applications, vol. 32, no. 20, pp. 15949–15963, 2020.

[8] S. Gite, A. Mishra, and K. Kotecha, “Enhanced lung image segmentation using deep learning,” Neural Computing and Applications, vol. 35, no. 31, pp. 22839–22853, 2023.

[9] J. Chen et al., “Dynamic mechanism-assisted artificial bee colony optimization for image segmentation of COVID-19 chest X-ray,” Displays, vol. 79, Art. no. 102485, 2023.

[10] T. Mahesh, M. Javeed, and D. Tiwary, “Internet of Things for health care mechanism,” International Journal of Research in Engineering, Science and Management, vol. 1, no. 9, pp. 1–6, Sep. 2018.

[11] A. Iqbal, M. Usman, and Z. Ahmed, “Tuberculosis chest X-ray detection using CNN-based hybrid segmentation and classification approach,” Biomedical Signal Processing and Control, vol. 84, Art. no. 104667, 2023.

[12] A. Sulaiman et al., “A convolutional neural network architecture for segmentation of lung diseases using chest X-ray images,” Diagnostics, vol. 13, no. 9, Art. no. 1651, 2023.

[13] S. R. Nayak et al., “An automated lightweight deep neural network for diagnosis of COVID-19 from chest X-ray images,” Arabian Journal for Science and Engineering, vol. 48, no. 8, pp. 11085–11102, 2023.

[14] G. M. M. Alshmrani, Q. Ni, R. Jiang, H. Pervaiz, and N. M. Elshennawy, “A deep learning architecture for multi-class lung diseases classification using chest X-ray images,” Alexandria Engineering Journal, vol. 64, pp. 923–935, 2023.

 DOI: 10.5281/zenodo.22755101

ISSN (Online): 2583-648X

IJIRID

International Journal of Ingenious Research, Invention and Development

An International, High Impact Factor, Double-Blind Peer-Reviewed, Open-Access, Multidisciplinary Online Journal

www.ijirid.in

Volume 5 | Issue 4 | August 2026

[15] R. K. Priya et al., "Fuzzy-entropic approach on chest X-ray region of interest segmentation-heart position shifting using differential evolution optimization and multi-level segmentation technique with cloud computing," Soft Computing, vol. 27, no. 3, pp. 1639–1650, 2023.

[16] S. Arvind, J. V. Tembhurne, T. Diwan, and P. Sahare, "Improvised light weight deep CNN based U-Net for the semantic segmentation of lungs from chest X-rays," Results in Engineering, vol. 17, Art. no. 100929, 2023.

[17] T. Srujana, D. Divya, and M. Javeed, "FPGA implementation for detection disease on cotton plants using advanced image processing algorithm," International Journal of Advanced Research in Electrical, Electronics and Instrumentation Engineering, vol. 7, no. 11, pp. 4023–4030, Nov. 2018.

[18] S. Rajaraman, F. Yang, G. Zamzmi, Z. Xue, and S. Antani, "Assessing the impact of image resolution on deep learning for TB lesion segmentation on frontal chest X-rays," Diagnostics, vol. 13, no. 4, Art. no. 747, 2023.

[19] B. R. dos Santos Silva et al., "Lung segmentation of chest X-rays using U-Net convolutional networks," in Computerized Systems for Diagnosis and Treatment of COVID-19, pp. 15–28, 2023.

[20] S. Hao et al., "Multi-threshold image segmentation using an enhanced fruit fly optimization for COVID-19 X-ray images," Biomedical Signal Processing and Control, Art. no. 105147, 2023.

[21] N. Gaggion et al., "CheXmask: A large-scale dataset of anatomical segmentation masks for multi-center chest X-ray images," arXiv preprint arXiv:2307.03293, 2023.

[22] H. Wang et al., "A multi-objective segmentation method for chest X-rays based on collaborative learning from multiple partially annotated datasets," Information Fusion, vol. 102, Art. no. 102016, 2024.

[23] D. Tiwary and M. Javeed, "Power management for low power VLSI design," International Journal of Creative Research Thoughts (IJCRT), vol. 6, no. 2, pp. 732–735, Apr. 2018.

[24] I. Ullah et al., "A deep learning based dual encoder–decoder framework for anatomical structure segmentation in chest X-ray images," Scientific Reports, vol. 13, Art. no. 791, 2023.

[25] X. Wu, J. Liang, Y. Zhang, and X. Tian, "A segmentation method based on PDNet for chest X-rays with targets in different positions and directions," Applied Sciences, vol. 13, no. 8, Art. no. 5000, 2023.

 DOI: 10.5281/zenodo.22755101